CLIMATOLOGY

# Accelerating rates of Arctic carbon cycling revealed by long-term atmospheric $CO_2$ measurements

Su-Jong Jeong[1]*, A. Anthony Bloom[2]*, David Schimel[2], Colm Sweeney[3,4], Nicholas C. Parazoo[2], David Medvigy[5], Gabriela Schaepman-Strub[6], Chunmiao Zheng[7], Christopher R. Schwalm[8,9], Deborah N. Huntzinger[10], Anna M. Michalak[11], Charles E. Miller[2]



**The contemporary Arctic carbon balance is uncertain, and the potential for a permafrost carbon feedback of anywhere from 50 to 200 petagrams of carbon (Schuur *et al.*, 2015) compromises accurate 21st-century global climate system projections. The 42-year record of atmospheric $CO_2$ measurements at Barrow, Alaska (71.29 N, 156.79 W), reveals significant trends in regional land-surface $CO_2$ anomalies ($\Delta CO_2$), indicating long-term changes in seasonal carbon uptake and respiration. Using a carbon balance model constrained by $\Delta CO_2$, we find a 13.4% decrease in mean carbon residence time (50% confidence range = 9.2 to 17.6%) in North Slope tundra ecosystems during the past four decades, suggesting a transition toward a boreal carbon cycling regime. Temperature dependencies of respiration and carbon uptake suggest that increases in cold season Arctic labile carbon release will likely continue to exceed increases in net growing season carbon uptake under continued warming trends.**

## INTRODUCTION

The Arctic has experienced unprecedented changes in recent decades (*1*), including rapid and diverse changes in Arctic ecosystems such as shrub cover expansion, enhanced vegetation productivity (Arctic greening), longer growing season, and permafrost thaw (*1*–*4*). These ecosystem changes influence rates of carbon cycling and the net Arctic carbon balance (*5*). For instance, increasing carbon release due to permafrost thaw or soil warming could significantly increase atmospheric $CO_2$ concentrations, whereas increasing carbon uptake due to enhanced Arctic vegetation productivity could significantly reduce atmospheric $CO_2$. In either case, Arctic carbon-climate feedbacks will drive global atmospheric $CO_2$ concentrations and alter Earth's climate trajectory (*6*).

Long-term atmospheric $CO_2$ surface measurements reveal an increase in the $CO_2$ seasonal amplitude in high latitudes (*7*), although it is unclear whether this increase is due to enhanced carbon uptake linked to increased productivity (*8*) or to accelerated decomposition of soil organic matter (*9*). With vast amounts of carbon stored in both the active layer and the underlying permafrost, an increase in soil carbon turnover could irreversibly transform the Arctic from a long-term sink to a long-term source (*10*–*12*). We hypothesize that climate change has increased both productivity and respiration and decreased the mean carbon residence time within Arctic ecosystems. Placing observational constraints on Arctic carbon residence time is therefore key to understanding the evolution of Arctic carbon balance and disentangling changes in productivity and respiration.

Direct measurements of pan-Arctic or regional northern high-latitude terrestrial carbon exchange are extremely challenging (*13*). Here, we place observational constraints on the tundra ecosystem carbon balance using the long-term atmospheric $CO_2$ record from Barrow, Alaska (*14*, *15*). We constrain the northern Alaska region (or "North Slope") land-atmosphere $CO_2$ exchange [that is, net ecosystem exchange (NEE)] for the period 1974–2015 by deconvolving background-influenced $CO_2$ variability from the Barrow $CO_2$ time series (see Materials and Methods). We treat monthly $CO_2$ anomalies ($\Delta CO_2$) as a proxy for North Slope regional-scale NEE. Following Commane *et al.* (*14*), we assume that background variations are predominantly influenced by large-scale ecosystems above 60°N, including tundra, boreal forest, and other Arctic ecosystems. We evaluate the long-term changes in intra- and interannual variations of $\Delta CO_2$ to characterize the long-term carbon dynamics over the Arctic regions. Here, negative (positive) $\Delta CO_2$ values indicate regional carbon uptake (release) relative to background $CO_2$.

## RESULTS AND DISCUSSION

We find a 0.04 ± 0.022 parts per million (ppm)/year ($P < 0.05$) increase in the seasonal amplitude of $\Delta CO_2$ (calculated as the annual maximum-to-minimum $\Delta CO_2$ difference) for the period 1974–2015 (Fig. 1, A and B). The increase in seasonal amplitude emerges mainly from an increasing early cold season (September and October) $\Delta CO_2$ (+0.031 ± 0.02 ppm/year, $P < 0.05$), combined partially with a decreasing early summer (June and July) $\Delta CO_2$ (−0.01 ± 0.01 ppm/year, $P < 0.5$) throughout the 42-year record. The observed amplification of seasonal $\Delta CO_2$ variability is consistent with observed changes in $CO_2$ seasonal amplitude in northern mid-latitudes (*7*). Previous studies attribute $\Delta CO_2$ amplitude changes to an increase in summertime carbon uptake by enhanced vegetation productivity (*8*) due to tundra greening (*3*), shrubification (*4*), a longer growing season (*16*), and northward migration of the boreal forest (*17*). However, these studies do not explicitly account for background $CO_2$ variability, which is dominated by $CO_2$ transport from low latitudes and imparts a phase delay in the seasonal $CO_2$ signal (*18*, *19*). Our results indicate that local changes in seasonal $CO_2$ amplitude are mainly due to early cold season respiration and that

[1]Department of Environmental Planning, Graduate School of Environmental Studies, Seoul National University, Seoul, Korea. [2]Jet Propulsion Laboratory, California Institute of Technology, Pasadena, CA 91109, USA. [3]Cooperative Institute for Research in Environmental Sciences, University of Colorado Boulder, Boulder, CO 80309, USA. [4]National Oceanic and Atmospheric Administration/Earth System Research Laboratory, Boulder, CO 80305, USA. [5]Department of Biological Sciences, University of Notre Dame, Notre Dame, IN 46556, USA. [6]Department of Evolutionary Biology and Environmental Studies, University of Zurich, Zurich, Switzerland. [7]School of Environmental Science and Engineering, Southern University of Science and Technology, Shenzhen, China. [8]Woods Hole Research Center, Falmouth, MA 02540, USA. [9]Center for Ecosystem Science and Society, Northern Arizona University, Flagstaff, AZ 86011, USA. [10]School of Earth Sciences and Environmental Sustainability, Northern Arizona University, Flagstaff, AZ 86011, USA. [11]Department of Global Ecology, Carnegie Institution for Science, Stanford, CA 94305, USA.
*Corresponding author. Email: sujong@snu.ac.kr (S.-J.J.); abloom@jpl.nasa.gov (A.A.B.)

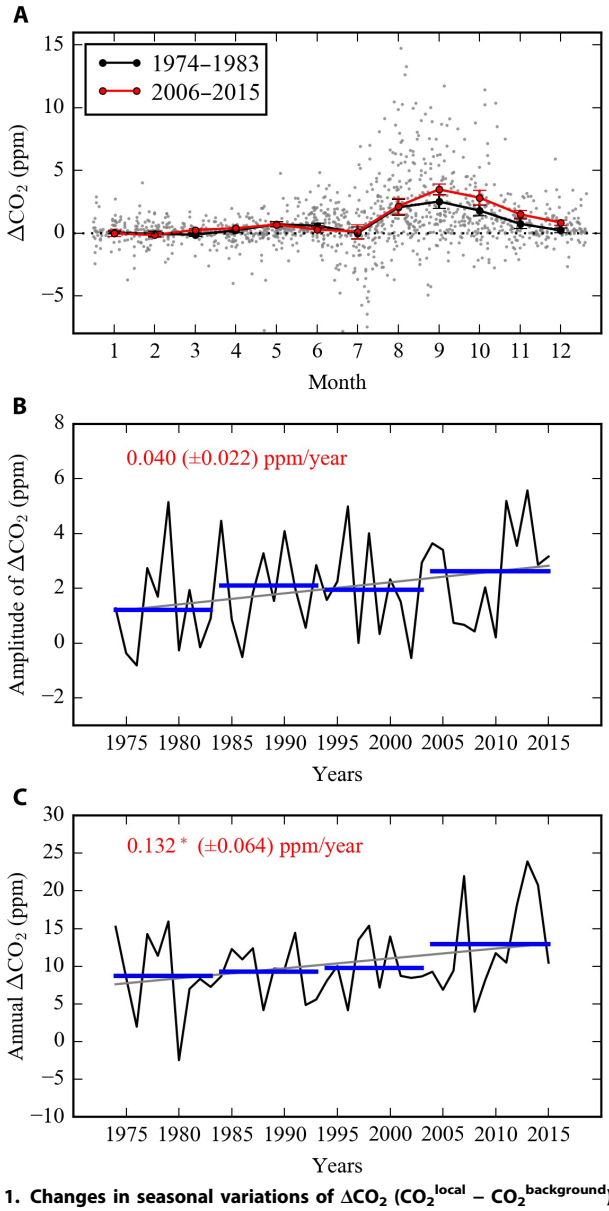


**Fig. 1. Changes in seasonal variations of $\Delta CO_2$ ($CO_2^{local} - CO_2^{background}$) for the last four decades (1974–2015).** (**A**) Monthly mean $\Delta CO_2$ for the period 1974–1983 and that for the period 2006–2015. (**B**) Changes in annual amplitude of $\Delta CO_2$ (maximum $\Delta CO_2$ − minimum $\Delta CO_2$). (**C**) Changes in annual $\Delta CO_2$ (sum of monthly $\Delta CO_2$). Gray dots in (A) show daily values of $\Delta CO_2$. The asterisk indicates statistical significance at the 95% confidence level.

nongrowing season $CO_2$ fluxes are an increasingly important component of the annual carbon balance (*9*, *14*).

We find that variations in early cold season $\Delta CO_2$ are strongly correlated to the soil temperature, especially in upper soil layers (0 to 40 cm; $P < 0.01$) (fig. S4). The positive relationship between near-surface soil temperature and $\Delta CO_2$ is consistent with anticipated soil carbon losses due to warming (*20*). In addition to early cold season warming, positive correlation between summertime (June, July, and August) averaged normalized difference vegetation index and early cold season (September to October) $\Delta CO_2$ shows a direct contribution of Arctic greening and increased productivity to early cold season $\Delta CO_2$ (fig. S5). This is consistent with a previous field study over the Arctic region (*21*), supporting the hypothesis that the increase in respiration of recent labile soil organic matter is proportional to the increase in carbon input by enhanced vegetation productivity (*22*, *23*).

In accordance with trends in seasonal $\Delta CO_2$, annual $\Delta CO_2$ exhibits a positive trend over the past 40 years (+0.132 ± 0.064 ppm/year, $P < 0.01$; Fig. 1C). Assuming that annual $\Delta CO_2$ is related to annual NEE, this result suggests that, despite the compensation between the increasing trends in carbon uptake (for example, negative trends in $\Delta CO_2$ during summer) and loss (for example, positive trend in $\Delta CO_2$ during early cold season), the mean carbon balance has significantly changed over time, given a stasis of seasonal changes in the wind speeds and boundary layer heights. Therefore, on the basis of 1974–2015 annual $\Delta CO_2$ trends, our results indicate that carbon release linked to increased soil thaw is increasing. However, given changes in the seasonal boundary layer height, it is difficult to assess whether soil carbon losses are outpacing carbon uptake due to enhanced vegetation productivity.

The carbon residence (or turnover) time is an emergent ecosystem property that diagnoses the interplay of climate, carbon fluxes, soil, and vegetation (*24*, *25*). Shorter residence times reflect ecosystems that can respond more rapidly to changing climate (*10*, *24*, *26*). Residence time depends on the intrinsic stability of the carbon stock and the environmentally limited (that is, soil temperature and moisture) rates of plant and microbial respiration (*27*, *28*). We evaluate integrated dynamics of northern Alaska carbon cycling by combining observed $\Delta CO_2$ and an ecosystem carbon balance model to retrieve the decadal trends in mean carbon residence time over Alaska. We use a Bayesian approach with observed $\Delta CO_2$ anomalies and an ecosystem carbon balance model (see Materials and Methods) and find a 99% probability that carbon residence time decreased throughout the study period. Mean carbon residence time for 2004–2013 is 13.4% lower than that for 1979–1988 (50% confidence interval, 9.2 to 17.6%, Fig. 2). In comparison, the Multi-scale Synthesis and Terrestrial Model Intercomparison Project (MsTMIP) ensemble of terrestrial biosphere models indicates a mean decrease of 8.8% (50% confidence interval, 5.0 to 12.8%; Fig. 2) in residence time for the same period (*29*). Although process-based models exhibit a weaker response, they do indicate a consistent decrease in carbon residence time across Arctic regions. In addition, our estimate for northern Alaska (50% confidence interval, 23 to 782 years; median, 139 years) is larger but broadly consistent with gridded residence time estimates (*24*) (range, 29 to 180 years; median, 55 years) and roughly an order of magnitude greater than tropical ecosystem mean residence times (*10*, *24*, *25*).

Our finding of a 13.4% decrease in the carbon residence time suggests that Alaska's North Slope tundra is becoming more boreal. A decrease in high-latitude residence time indicates an increased sensitivity of Arctic carbon cycling to warming and, therefore, an enhanced role of Arctic ecosystems in the variability of atmospheric $CO_2$. Although several processes can contribute to residence time changes, we hypothesize that residence time changes are occurring as a result of changes in dead organic carbon turnover rates and/or trends in the live biomass/dead organic carbon ratio. Carbon held in permafrost is effectively permanently stored, with a minuscule decomposition rate; therefore, permafrost thaw transfers carbon to a far more active phase and effectively reduces the average carbon residence time. Shrubification and forest migration would likely lead to higher carbon allocation to long-lived woody carbon pools (*30*), therefore leading to a likely increase or no change in the residence time of live biomass. However, biomass accumulation due to shrubification would lead to a higher live biomass/dead organic carbon ratio, leading to a decrease in mean ecosystem carbon residence

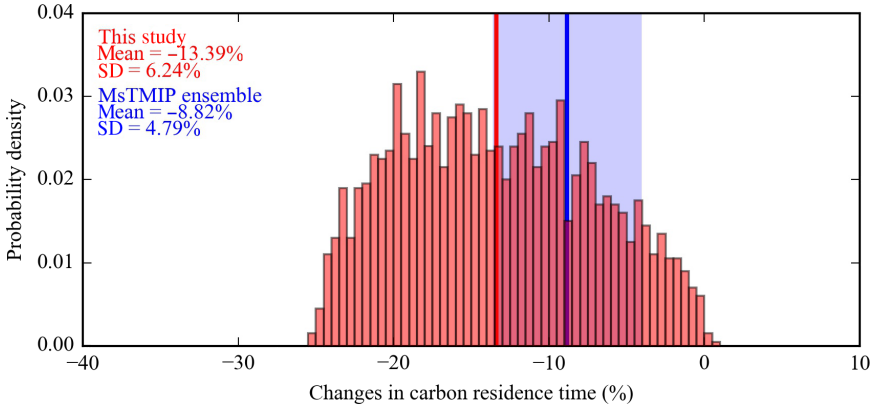


**Fig. 2. Retrieved changes in carbon residence time based on the difference between 1979–1988 and 2004–2013 10-year periods.** The vertical red line indicates the average of retrieved changes in carbon residence time. The blue line indicates mean (solid line) and range (shading) in the equivalent residence time change estimates from the MsTMIP model ensemble.

time, since live biomass residence times are roughly an order of magnitude lower than those of dead organic carbon matter (*31*).

Our analysis also indicates a 54% probability that soil (heterotrophic) respiration is more temperature-sensitive than net carbon uptake (fig. S3), resolving a key uncertainty in the response of Arctic ecosystems to climate change. The enhanced response of soil decomposition and respiration to warming and deepening of the soil active layer implies net ecosystem carbon loss under elevated temperatures in the 21st century. To gain confidence in the sensitivity of carbon respiration and uptake to climatic variability, the effects of permafrost mobilization and priming (*32*), biomass accumulation, and subsequent shifts in live biomass inputs into dead organic carbon pools need to be explored further; however, these processes will likely contribute to a sustained or increasing future net carbon loss from Arctic ecosystems. Soil moisture and precipitation trends will likely influence the rate of permafrost degradation, decomposition rates, and the $CO_2$:$CH_4$ of heterotrophically respired carbon (*33*); these carbon-water relationships remain uncertain and highlight the need for an improved understanding of the integrated long-term carbon dynamics and carbon balance sensitivity to hydrological variability in the Arctic system (*1*).

Observationally constrained carbon residence time estimates can help narrow uncertainties of carbon cycle predictions (*34*) and improve understanding of Arctic carbon-climate feedbacks. Absolute $CO_2$ flux constraints based on past and current $CO_2$ observation systems will ultimately help resolve the processes controlling long-term variations in terrestrial carbon exchanges. We anticipate that regional top-down constraints on ecosystem carbon cycling—including atmospheric $CO_2$ flux constraints (*35*), such as satellite, airborne, and tower solar-induced fluorescence (*36*, *37*), and land-surface data constraints (*25*)—will together provide an enhanced process understanding of Arctic terrestrial carbon cycling sensitivity and vulnerability to long-term climate trends.

## MATERIALS AND METHODS

### Regional land attributions of observed $CO_2$ anomalies ($\Delta CO_2$)

We used half-hourly $CO_2$ concentration measurements at Barrow, Alaska, from the National Oceanic and Atmospheric Administration (NOAA) Earth System Research Laboratory archive for the period 1974–2015 (*38*). We discriminated between local $CO_2$ ($CO_2^{local}$) and background $CO_2$ concentrations ($CO_2^{background}$) based on wind direction, wind speed, and time of day (*14*, *15*). Sweeney *et al.* (*15*) applied the method to separate land sources of $CH_4$ from the clean air sector. Commane *et al.* (*14*) verified this method to estimate land sources of observed $CO_2$ at Barrow by using the Hybrid Single-Particle Lagrangian Integrated Trajectory Model driven by meteorological data from NOAA. Locally influenced $CO_2$ concentrations ($CO_2^{local}$) were derived on the basis of 12:00 p.m. to 4:00 p.m. half-hourly $CO_2$ measurements where wind speed exceeded 3 m/s and wind direction was between 150° and 210°. Background $CO_2$ concentrations ($CO_2^{background}$) were derived on the basis of 12:00 p.m. to 4:00 p.m. half-hourly $CO_2$ measurements where wind speed exceeded 3 m/s and wind direction was between 0° and 90°. Finally, we defined local attributions of $CO_2$ changes as $\Delta CO_2 = CO_2^{local} - CO_2^{background}$. More details in this method are described in Commane *et al.* (*14*) and Sweeney *et al.* (*15*).

We selected data from 12:00 p.m. to 4:00 p.m. during the day because boundary layer height is the highest during this time. A higher boundary layer expands the surface area of influence significantly, resulting in a larger volume of air that is mixed from the surface to the top of the boundary layer. Thus, air that may have been at the surface a day ago but has escaped the nighttime boundary layer can be reincorporated during this time of the day. As the boundary layer stratifies during other times of the day, the area of influence is significantly reduced, making the change from background more local. It should also be noted that, because boundary layer is higher between 12:00 p.m. and 4:00 p.m. than any other time of the day, it will also be more diluted by the overlying free tropospheric air that sits over the boundary layer.

Daily measurements show a mix of negative and positive anomalies ($\Delta CO_2$) over the first and last decades of our study (1974–1983 and 2006–2015, respectively; Fig. 1). However, on average, monthly $\Delta CO_2$ are predominantly positive over the course of the year. This pattern is mainly due to the limited duration of the drawdown period and variability of that period from year to year, making the monthly average positive despite many negative daily observations. It also should be noted that the delayed growing season drawdown in tundra (summer) relative to southern boreal and temperate forests (spring) will result in pan-Arctic "background" $CO_2$ significantly depleted relative to that observed at Barrow (*15*, *18*).

### Model-data fusion

We retrieved the change in ecosystem carbon residence time by assimilating June and September 1979–2015 $\Delta CO_2$ into a single-pool ecosystem carbon balance model. We used a Bayesian model-data fusion approach (*25*) to optimize five model parameters relating to carbon uptake, initial ecosystem carbon stock, turnover rate, and the temperature sensitivities of carbon uptake and respiration. We used a Metropolis-Hastings Markov Chain Monte Carlo algorithm to sample 5000 model parameter sets. We evaluated the model results against a process-based terrestrial biosphere model ensemble (*29*), flux tower–based estimates of carbon uptake (*36*), and residence time retrievals (*24*, *25*).

In the following sections, we describe the optimization of a first-order ecosystem carbon balance model scheme for the period 1979–2015. The temporal change in mean ecosystem C residence time—and its associated uncertainty—is derived on the basis of the optimized model output.

### Ecosystem carbon balance model

We expressed the total active terrestrial ecosystem carbon $C$ within the northern Alaska region (longitude, 170°W to 150°W; latitude, 65°N to 70°N) at time $t + 1$ as

$$C_{t+1} = C_t + \Delta t(\mathrm{NPP}_t - R_t) \quad (1)$$

where $\mathrm{NPP}_t$ is the net primary productivity, $R_t$ is the heterotrophic respiration, and $\Delta t$ is the time step. We represent the first-order sensitivity of $\mathrm{NPP}_t$ to temperature ($T_t$), leaf area index ($\mathrm{LAI}_t$), and global radiation ($S_t$) as follows

$$\mathrm{NPP}_t = p_1 S_t \mathrm{LAI}_t\, p_2^{\frac{T_t}{10}} \quad (2)$$

where $p_1$ is a baseline productivity parameter and $p_2$ is an exponential temperature dependence parameter. $S_t$ and $T_t$ (2-m air temperature) data were derived from ERA-interim 1979–2015 1° × 1° reanalysis fields. $\mathrm{LAI}_t$ was obtained from Zhu *et al.* (*16*). $R_t$ was derived as a function of temperature, where

$$R_t = C_t\, p_3\, p_4^{\frac{T_t}{10}} \quad (3)$$

where $p_3$ is a baseline turnover rate and $p_4$ is an exponential temperature dependence parameter. At each time step, the $\mathrm{NEE}_t$ is

$$\mathrm{NEE}_t = R_t - \mathrm{NPP}_t \quad (4)$$

Our model is a first-order representation of the integrated ecosystem carbon dynamics and their sensitivity to leaf area, solar radiation, and temperature. We noted that our NPP derivation assumes (i) no hydrological limitations on carbon uptake in Arctic ecosystems, (ii) a linear relationship with respect to LAI and $S_t$, and (iii) respiration dependence on the 2-m air temperature (instead of surface or subsurface temperature). We determined the viability of our approach by comparing northern Alaska–optimized monthly $\mathrm{NPP}_t$ against a range of process-based terrestrial biosphere models (*29*, *39*). The optimization of model parameters and the comparison of our model with process-based models are described in the following section. Our model assumes that carbon losses due to disturbance are a minimal component of the Alaska North Slope carbon balance: Land management and land-use change are minimal components of the Arctic ecosystem carbon cycling, while mean C fire emissions (based on the global fire emission database, version 4) (*40*) account for <0.19 grams of carbon (gC) $m^{-2}$ $month^{-1}$ for the period 2001–2013, roughly two orders of magnitude smaller than mean uptake and respiration fluxes (see fig. S2).

### Model optimization

We optimized model parameters based on 1979–2013 monthly $\Delta CO_2$ observations; we henceforth referred to model parameters—$p_1$, $p_2$, $p_3$, $p_4$, and $C_0$—as $\mathbf{x}$ and to monthly $\Delta CO_2$ observations as $\mathbf{O}$. We used Bayesian inference to derive the probability distribution of $\mathbf{x}$ relative to observational constraints $\mathbf{O}$, $\mathbf{p}(\mathbf{x}|\mathbf{O})$, where

$$\mathbf{p}(\mathbf{x}|\mathbf{O}) \propto \mathbf{p}(\mathbf{O}|\mathbf{x})\mathbf{p}(\mathbf{x}) \quad (5)$$

$\mathbf{p}(\mathbf{x})$ is the prior probability of $\mathbf{x}$, and $\mathbf{p}(\mathbf{O}|\mathbf{x})$ is the likelihood of $\mathbf{x}$ given $\mathbf{O}$. We used a Markov Chain Monte Carlo approach (*41*) to extract 5000 samples of $\mathbf{x}$. In addition to broad uniform prior parameter ranges (table S1), we (i) prescribed a 10 gC $m^{-2}$ $month^{-1}$ constraint on mean annual NPP with a factor of 2 uncertainty, which is broadly consistent with the MsTMIP [BG1 simulations, comparison in fig. S2; see Materials and Methods (Comparison with process-based terrestrial biosphere model ensemble) for MsTMIP experiment details], and (ii) ensured that |NEE| is statistically within 1 SD of mean NPP. Hence, for each Monte Carlo iteration, the prior probability of parameter sample $\mathbf{x}_n$, $\mathbf{p}(\mathbf{x}_n)$, is evaluated as

$$\mathbf{p}(\mathbf{x}_n) = \mathbf{p}_{\mathrm{range}}(\mathbf{x}_n) e^{-\frac{1}{2}\left(\frac{\log\left(\frac{\overline{\mathrm{NPP}}(\mathbf{x}_n)}{\mathrm{NPP}_0}\right)}{\log(2)}\right)^2} e^{-\frac{1}{2}\left(\frac{\overline{\mathrm{NEE}}(\mathbf{x}_n)}{\overline{\mathrm{NPP}}(\mathbf{x}_n)}\right)^2} \quad (6)$$

where $\mathbf{p}_{\mathrm{range}}(\mathbf{x}_n)$ is 1 if $\mathbf{x}$ is within the prior parameter ranges (or zero otherwise), $\overline{\mathbf{NPP}}(\mathbf{x}_n)$ and $\overline{\mathbf{NEE}}(\mathbf{x}_n)$ are the mean model NPP and NEE for the period 1979–2013, respectively (derived as shown in Eqs. 2 and 4), and $\mathrm{NPP}_0$ = 10 gC $m^{-2}$ $month^{-1}$. We defined the likelihood of $\mathbf{x}_n$ given observational constraints $\Delta CO_2$ as

$$\mathbf{p}(\mathbf{O}|\mathbf{x}_n) = e^{-\frac{1}{2}\left(\frac{\mathbf{nee}_m(\mathbf{x}_n) - \mathbf{a}_m}{\sigma_m}\right)^2} \quad (7)$$

where $\mathbf{nee}_m$ and $\mathbf{a}_m$ are the vectors of monthly NEE and $\Delta CO_2$ standardized anomalies for month $m$, respectively. For each $m$, standardized anomalies $\mathbf{nee}_m$ ($\mathbf{a}_m$) were derived by removing mean 1979–2013 NEE ($\Delta CO_2$). We hence assumed a linear relationship between $\Delta CO_2$ and NEE for each month. By standardizing monthly anomalies independently, we did not assume that monthly $\Delta CO_2$ anomalies were comparable. For each month, the model-data residual ($\mathbf{nee}_m - \mathbf{a}_m$) was weighed by uncertainty $\sigma_m$. We weighed the model-data residuals ($\mathbf{nee}_m - \mathbf{a}_m$) by $\sigma_m$ = 10 SD($\mathbf{a}_m$), where SD($\mathbf{a}_m$) represents the SD of the bracketed vector. We noted that the uncertainty and error covariance structure of $\mathbf{a}_m$ and the representation error of $\mathbf{nee}_m$ are largely unknown: To avoid overconstraining the model, we chose to prescribe $\sigma_m$ = 10 SD($\mathbf{a}_m$), since we found that prescribing $\sigma_m$ < 10 SD($\mathbf{a}_m$) did increase model confidence but without a substantial reduction in model-data residuals.

Standardized observations and optimized standardized model NEE are shown in fig. S1. The details of the Metropolis-Hastings Markov

Chain Monte Carlo algorithm are described in Bloom and Williams (*41*) and references therein. Both model NPP and heterotrophic respiration peak in July, which is consistent with half (four of eight) of the MsTMIP terrestrial biosphere models (fig. S2).

### Retrieved residence time change and temperature sensitivities

We derived the percentage of residence time change ($\Delta\tau$) as follows

$$\Delta\tau = \left(\frac{\tau_{end}}{\tau_{start}} - 1\right) \times 100\% \quad (8)$$

where $\tau_{start}$ and $\tau_{end}$ correspond to the mean ecosystem C residence times based on the 1979–1988 and 2004–2013 10-year periods. The residence time is derived in accordance with Bloom *et al.* (*25*), where each $\tau$ is derived as

$$\tau = \frac{\overline{C}}{\overline{R}} \quad (9)$$

where $\overline{C}$ and $\overline{R}$ are the 10-year mean C stocks and heterotrophic respirations, respectively, for the corresponding $\tau$ time spans. The range of $\Delta\tau$ values is derived by repeating Eq. 8 for each model parameter vector sample $\mathbf{x}_n$. On the basis of $\Delta\tau$ outcomes for all accepted parameter vectors, we found that the probability of $\Delta\tau < 0$ is 99%. The distribution of the optimized temperature sensitivities of NPP and $R$ (parameters $p_2$ and $p_4$; table S1) is shown in fig. S3. On the basis of all accepted parameter vector samples $\mathbf{x}$, we found that the probability of $p_4 > p_2$ is 54%.

### Comparison with process-based terrestrial biosphere model ensemble

We compared the ecosystem carbon balance model NPP, heterotrophic respiration, and retrieved mean residence times with the MsTMIP terrestrial biosphere model ensemble outputs [V1.0 MsTMIP outputs (*39*)]. To compare model C residence times (see section S4), we limited our comparison to BG1 simulation models in MsTMIP, which provided both heterotrophic respiration and total soil carbon outputs (table S2): We noted that since $\tau$ is dependent on total modeled C stocks and fluxes during a certain time period, it provides a complexity-independent first-order metric of the rate at which C is cycled through the terrestrial biosphere. The BG1 simulations include time-varying climate, nitrogen deposition, atmospheric $CO_2$, and land-use history: For the sake of brevity, we refer the reader to Huntzinger *et al.* (*29*) for individual model details.

## SUPPLEMENTARY MATERIALS

Supplementary material for this article is available at http://advances.sciencemag.org/cgi/content/full/4/7/eaao1167/DC1

Table S1. Prior parameter value ranges.

Table S2. MsTMIP models in this study (BG1 simulations).

Fig. S1. Comparison between simulated NEE and observed $\Delta CO_2$.

Fig. S2. Comparison of net primary productivity and heterotrophic respiration between optimized model and MsTMIP terrestrial biosphere models.

Fig. S3. Posterior probability distribution of the ratio of effective $Q_{10}$ temperature sensitivity parameters $p_2$ (NPP) and $p_4$ (Rhet) [see Materials and Methods (Retrieved residence time change and temperature sensitivities) and table S1 for details].

Fig. S4. Relationships between $\Delta CO_2$ and soil temperature (0 to 40 cm).

Fig. S5. Lagged (0 to 3 months) relationships between summertime vegetation greenness and autumn $\Delta CO_2$.

References (*42*, *43*)

## REFERENCES AND NOTES


1. L. D. Hinzman, C. J. Deal, A. D. McGuire, S. H. Mernild, I. V. Polyakov, J. E. Walsh, Trajectory of the Arctic as an integrated system. *Ecol. Appl.* **23**, 1837–1868 (2013).
2. M. C. Serreze, J. E. Walsh, F. S. Chapin III, T. Osterkamp, M. Dyurgerov, V. Romanovsky, W. C. Oechel, J. Morison, T. Zhang, R. G. Barry, Observational evidence of recent change in the northern high-latitude environment. *Clim. Change* **46**, 159–207 (2000).
3. U. S. Bhatt, D. A. Walker, M. K. Raynolds, J. C. Comiso, H. E. Epstein, G. Jia, R. Gens, J. E. Pinzon, C. J. Tucker, C. E. Tweedie, P. J. Webber, Circumpolar Arctic tundra vegetation change is linked to sea ice decline. *Earth Interact* **14**, 1–20 (2010).
4. I. H. Myers-Smith, S. C. Elmendorf, P. S. A. Beck, M. Wilmking, M. Hallinger, D. Blok, K. D. Tape, S. A. Rayback, M. Macias-Fauria, B. C. Forbes, J. D. M. Speed, N. Boulanger-Lapointe, C. Rixen, E. Lévesque, N. M. Schmidt, C. Baittinger, A. J. Trant, L. Hermanutz, L. S. Collier, M. A. Dawes, T. C. Lantz, S. Weijers, R. H. Jørgensen, A. Buchwal, A. Buras, A. T. Naito, V. Ravolainen, G. Schaepman-Strub, J. A. Wheeler, S. Wipf, K. C. Guay, D. S. Hik, M. Vellend, Climate sensitivity of shrub growth across the tundra biome. *Nat. Clim. Chang.* **5**, 887–891 (2015).
5. A. D. McGuire, T. R. Christensen, D. Hayes, A. Heroult, E. Euskirchen, J. S. Kimball, C. Koven, P. Lafleur, P. A. Miller, W. Oechel, P. Peylin, M. Williams, Y. Yi, An assessment of the carbon balance of Arctic tundra: Comparisons among observations, process models, and atmospheric inversions. *Biogeosciences* **9**, 3185–3204 (2012).
6. P. Friedlingstein, M. Meinshausen, V. K. Arora, C. D. Jones, A. Anav, S. K. Liddicoat, R. Knutti, Uncertainties in CMIP5 climate projections due to carbon cycle feedbacks. *J. Climate* **27**, 511–516 (2015).
7. H. D. Graven, R. F. Keeling, S. C. Piper, P. K. Patra, B. B. Stephens, S. C. Wofsy, L. R. Welp, C. Sweeney, P. P. Tans, J. J. Kelley, B. C. Daube, E. A. Kort, G. W. Santoni, J. D. Bent, Enhanced seasonal exchange of $CO_2$ by northern ecosystems since 1960. *Science* **341**, 1085–1089 (2013).
8. M. Forkel, N. Carvalhais, C. Rödenbeck, R. Keeling, M. Heimann, K. Thonicke, S. Zaehle, M. Reichstein, Enhanced seasonal $CO_2$ exchange caused by amplified plant productivity in northern ecosystems. *Science* **351**, 696–699 (2016).
9. S. Piao, P. Ciais, P. Friedlingstein, P. Peylin, M. Reichstein, S. Luyssaert, H. Margolis, J. Fang, A. Barr, A. Chen, A. Grelle, D. Y. Hollinger, T. Laurila, A. Lindroth, A. D. Richardson, T. Vesala, Net carbon dioxide losses of northern ecosystems in response to autumn warming. *Nature* **451**, 49–52 (2008).
10. A. D. Friend, W. Lucht, T. T. Rademacher, R. Keribin, R. Betts, P. Cadule, P. Ciais, D. B. Clark, R. Dankers, P. D. Falloon, A. Ito, R. Kahana, A. Kleidon, M. R. Lomas, K. Nishina, S. Ostberg, R. Pavlick, P. Peylin, S. Schaphoff, N. Vuichard, L. Warszawski, A. Wiltshire, F. I. Woodward, Carbon residence time dominates uncertainty in terrestrial vegetation responses to future climate and atmospheric $CO_2$. *Proc. Natl. Acad. Sci. U.S.A.* **111**, 3280–3285 (2014).
11. E. F. Belshe, E. A. G. Schuur, B. M. Bolker, Tundra ecosystems observed to be $CO_2$ sources due to differential amplification of the carbon cycle. *Ecol. Lett.* **16**, 1307–1315 (2013).
12. Y. He, S. E. Trumbore, M. S. Torn, J. W. Harden, L. J. S. Vaughn, S. D. Allison, J. T. Randerson, Radiocarbon constraints imply reduced carbon uptake by soils during the 21st century. *Science* **353**, 1419–1424 (2016).
13. D. Shimel, R. Pavlick, J. B. Fisher, G. P. Asner, S. Saatchi, P. Townsend, C. Miller, C. Frankenberg, K. Hibbard, P. Cox, Observing terrestrial ecosystems and the carbon cycle from space. *Glob. Chang. Biol.* **21**, 1762–1776 (2015).
14. R. Commane, J. Lindaas, J. Benmergui, K. A. Luus, R. Y.-W. Chang, B. C. Daube, E. S. Euskirchen, J. M. Henderson, A. Karion, J. B. Miller, S. M. Miller, N. C. Parazoo, J. T. Randerson, C. Sweeney, P. Tans, K. Thoning, S. Veraverbeke, C. E. Miller, S. C. Wofsy, Carbon dioxide sources from Alaska driven by increasing early winter respiration from Arctic tundra. *Proc. Natl. Acad. Sci. U.S.A.* **114**, 5361–5366 (2017).
15. C. Sweeney, E. Dlugokencky, C. E. Miller, S. Wofsy, A. Karion, S. Dinardo, R. Y.-W. Chang, J. B. Miller, L. Bruhwiler, A. M. Crotwell, T. Newberger, K. McKain, R. S. Stone, S. E. Wolter, P. E. Lang, P. Tans, No significant increase in long-term $CH_4$ emissions on North Slope of Alaska despite significant increase in air temperature. *Geophys. Res. Lett.* **43**, 6604–6611 (2016).
16. Z. Zhu, R. B. Myneni, M. Huang, Z. Zeng, J. G. Canadell, P. Ciais, S. Sitch, P. Friedlingstein, A. Arneth, C. Cao, L. Cheng, E. Kato, C. Koven, Y. Li, X. Lian, Y. Liu, R. Liu, J. Mao, Y. Pan, S. Peng, J. Peñuelas, B. Poulter, T. A. M. Pugh, B. D. Stocker, N. Viovy, X. Wang, Y. Wang, Z. Xiao, H. Yang, S. Zaehle, N. Zeng, Greening of the Earth and its drivers. *Nat. Clim. Chang.* **6**, 791–795 (2016).
17. R. G. Pearson, S. J. Phillips, M. M. Loranty, P. S. A. Beck, T. Damoulas, S. J. Knight, S. J. Goetz, Shifts in Arctic vegetation and associated feedbacks under climate change. *Nat. Clim. Chang.* **3**, 673–677 (2013).

18. N. C. Parazoo, R. Commane, S. C. Wofsy, C. D. Koven, C. Sweeney, D. M. Lawrence, J. Lindaas, R. Y. Chang, C. E. Miller, Detecting regional patterns of changing $CO_2$ flux in Alaska. *Proc. Natl. Acad. Sci. U.S.A.* **113**, 7733–7738 (2016).
19. E. A. Barnes, N. C. Parazoo, C. Orbe, A. S. Denning, Isentropic transport and the seasonal cycle amplitude of $CO_2$. *J. Geophys. Res. Atmos.* **121**, 8106–8124 (2016).
20. T. W. Crowther, K. E. O. Todd-Brown, C. W. Rowe, W. R. Wieder, J. C. Carey, M. B. Machmuller, B. L. Snoek, S. Fang, G. Zhou, S. D. Allison, J. M. Blair, S. D. Bridgham, A. J. Burton, Y. Carrillo, P. B. Reich, J. S. Clark, A. T. Classen, F. A. Dijkstra, B. Elberling, B. A. Emmett, M. Estiarte, S. D. Frey, J. Guo, J. Harte, L. Jiang, B. R. Johnson, G. Kröel-Dulay, K. S. Larsen, H. Laudon, J. M. Lavallee, Y. Luo, M. Lupascu, L. N. Ma, S. Marhan, A. Michelsen, J. Mohan, S. Niu, E. Pendall, J. Peñuelas, L. Pfeifer-Meister, C. Poll, S. Reinsch, L. L. Reynolds, I. K. Schmidt, S. Sistla, N. W. Sokol, P. H. Templer, K. K. Treseder, J. M. Welker, M. A. Bradford, Quantifying global soil carbon losses in response to warming. *Nature* **540**, 104–108 (2016).
21. T. C. Parker, J.-A. Subke, P. A. Wookey, Rapid carbon turnover beneath shrub and tree vegetation is associated with low soil carbon stocks at a subarctic treeline. *Glob. Chang. Biol.* **21**, 2070–2081 (2015).
22. C. M. Litton, J. W. Raich, M. G. Ryan, Carbon allocation in forest ecosystems. *Glob. Chang. Biol.* **13**, 2089–2109 (2007).
23. D. B. Metcalfe, R. A. Fisher, D. A. Wardle, Plant communities as drivers of soil respiration: Pathways, mechanisms, and significance for global change. *Biogeosciences* **8**, 2047–2061 (2011).
24. N. Carvalhais, M. Forkel, M. Khomik, J. Bellarby, M. Jung, M. Migliavacca, M. Mu, S. Saatchi, M. Santoro, M. Thurner, U. Weber, B. Ahrens, C. Beer, A. Cescatti, J. T. Randerson, M. Reichstein, Global covariation of carbon turnover times with climate in terrestrial ecosystems. *Nature* **514**, 213–217 (2014).
25. A. A. Bloom, J. F. Exbrayat, I. R. van der Velde, L. Feng, M. Williams, The decadal state of the terrestrial carbon cycle: Global retrievals of terrestrial carbon allocation, pools, and residence times. *Proc. Natl. Acad. Sci. U.S.A.* **113**, 1285–1290 (2016).
26. S. E. Trumbore, O. A. Chadwick, R. Amundson, Rapid exchange between soil carbon and atmospheric carbon dioxide driven by temperature change. *Science* **272**, 393–396 (1996).
27. D. Schimel, R. Braswell, E. A. Holland, R. McKeown, D. S. Ojima, T. H. Painter, W. J. Parton, A. R. Townsend, Climatic, edaphic, and biotic controls over storage and turnover of carbon in soils. *Glob. Biogeochem. Cycles* **8**, 279–293 (1994).
28. M. W. I. Schmidt, M. S. Torn, S. Abiven, T. Dittmar, G. Guggenberger, I. A. Janssens, M. Kleber, I. Kögel-Knabner, J. Lehmann, D. A. C. Manning, P. Nannipieri, D. P. Rasse, S. Weiner, S. E. Trumbore, Persistence of soil organic matter as an ecosystem property. *Nature* **478**, 49–56 (2011).
29. D. N. Huntzinger, C. Schwalm, A. M. Michalak, K. Schaefer, A. W. King, Y. Wei, A. Jacobson, S. Liu, R. B. Cook, W. M. Post, G. Berthier, D. Hayes, M. Huang, A. Ito, H. Lei, C. Lu, J. Mao, C. H. Peng, S. Peng, B. Poulter, D. Riccuito, X. Shi, H. Tian, W. Wang, N. Zeng, F. Zhao, Q. Zhu, The North American Carbon Program Multi-scale Synthesis and Terrestrial Model Intercomparison Project—Part 1: Overview and experimental design. *Geosci. Model Dev.* **6**, 2121–2133 (2013).
30. S. C. Elmendorf, G. H. Henry, R. D. Hollister, R. G. Björk, A. D. Bjorkman, T. V. Callaghan, L. S. Collier, E. J. Cooper, J. H. Cornelissen, T. A. Day, A. M. Fosaa, W. A. Gould, J. Grétarsdóttir, J. Harte, L. Hermanutz, D. S. Hik, A. Hofgaard, F. Jarrad, I. S. Jónsdóttir, F. Keuper, K. Klanderud, J. A. Klein, S. Koh, G. Kudo, S. I. Lang, V. Loewen, J. L. May, J. Mercado, A. Michelsen, U. Molau, I. H. Myers-Smith, S. F. Oberbauer, S. Pieper, E. Post, C. Rixen, C. H. Robinson, N. M. Schmidt, G. R. Shaver, A. Stenström, A. Tolvanen, O. Totland, T. Troxler, C. H. Wahren, P. J. Webber, J. M. Welker, P. A. Wookey, Global assessment of experimental climate warming on tundra vegetation: Heterogeneity over space and time. *Ecol. Lett.* **15**, 164–175 (2012).
31. T. J. Zamin, M. S. Bret-Harte, P. Grogan, Evergreen shrubs dominate responses to experimental summer warming and fertilization in Canadian mesic low Arctic tundra. *J. Ecol.* **102**, 749–766 (2014).
32. K. Gerogiou, C. D. Koven, W. J. Riley, M. S. Torn, Toward improved model structures for analyzing priming: Potential pitfalls of using bulk turnover time. *Glob. Chang. Biol.* **21**, 4298–4302 (2015).
33. E. A. G. Schuur, A. D. McGuire, C. Schädel, G. Grosse, J. W. Harden, D. J. Hayes, G. Hugelius, C. D. Koven, P. Kuhry, D. M. Lawrence, S. M. Natali, D. Olefeldt, V. E. Romanovsky, K. Schaefer, M. R. Turetsky, C. C. Treat, J. E. Vonk, Climate change and the permafrost carbon feedback. *Nature* **520**, 171–179 (2015).
34. C. D. Koven, J. Q. Chambers, K. Georgiou, R. Knox, R. Negron-Juarez, W. J. Riley, V. K. Arora, V. Brovkin, P. Friedlingstein, C. D. Jones, Controls on terrestrial carbon feedbacks by productivity versus turnover in the CMIP5 Earth system models. *Biogeosciences* **12**, 5211–5228 (2015).
35. J. M. Henderson, J. Eluszkiewicz, M. E. Mountain, T. Nehrkorn, R. Y.-W. Chang, A. Karion, J. B. Miller, C. Sweeney, N. Steiner, S. C. Wofsy, C. E. Miller, Atmospheric transport simulations in support of the Carbon in Arctic Reservoirs Vulnerability Experiment (CARVE). *Atmos. Chem. Phys.* **15**, 4093–4116 (2015).
36. K. A. Luus, R. Commane, N. C. Parazoo, J. Benmergui, E. S. Euskirchen, C. Frankenberg, J. Joiner, J. Lindaas, C. E. Miller, W. C. Oechel, D. Zona, S. Wofsy, J. C. Lin, Tundra photosynthesis captured by satellite-observed solar-induced chlorophyll fluorescence. *Geophys. Res. Lett.* **44**, 1564–1573 (2017).
37. Y. P. Shiga, J. M. Tadić, X. Qiu, V. Yadav, A. E. Andrews, J. A. Berry, A. M. Michalak, Atmospheric $CO_2$ observations reveal strong correlation between regional net biospheric carbon uptake and solar-induced chlorophyll fluorescence. *Geophys. Res. Lett.* **45**, 1122–1132 (2018).
38. K. W. Thoning, D. R. Kitzis, A. Crotwell, Atmospheric carbon dioxide dry air mole fractions from quasi-continuous measurements at Barrow, Alaska, version 2015-12 (updated annually) [National Oceanic and Atmospheric Administration (NOAA), Earth System Research Laboratory (ESRL), Global Monitoring Division (GMD), 2015]; http://dx.doi.org/10.7289/V5RR1W6B.
39. D. N. Huntzinger, C. R. Schwalm, Y. Wei, R. B. Cook, A. M. Michalak, K. Schaefer, A. R. Jacobson, M. A. Arain, P. Ciais, J. B. Fisher, D. J. Hayes, M. Huang, S. Huang, A. Ito, A. K. Jain, H. Lei, C. Lu, F. Maignan, J. Mao, N. C. Parazoo, C. Peng, S. Peng, B. Poulter, Q. Zhu, NACP MsTMIP: Global 0.5-deg Terrestrial Biosphere Model Outputs (version1) in standard format, data set (Oak Ridge National Laboratory Distributed Active Archive Center, 2015).
40. G. R. van der Werf, J. T. Randerson, L. Giglio, G. J. Collatz, M. Mu, P. S. Kasibhatla, D. C. Morton, R. S. DeFries, Y. Jin, T. T. van Leeuwen, Global fire emissions and the contribution of deforestation, savanna, forest, agricultural, and peat fires (1997–2009). *Atmos. Chem. Phys.* **10**, 11707–11735 (2010).
41. A. A. Bloom, M. Williams, Constraining ecosystem carbon dynamics in a data-limited world: Integrating ecological "common sense" in a model–data fusion framework. *Biogeosciences* **12**, 1299–1315 (2015).
42. National Centers for Environmental Prediction/National Weather Service/NOAA/U.S. Department of Commerce, NCEP North American Regional Reanalysis (NARR) 2005, updated monthly (Research Data Archive at the National Center for Atmospheric Research, Computational and Information Systems Laboratory, 2016); http://rda.ucar.edu/datasets/ds608.0/.
43. J. E. Pinzon, C. J. Tucker, A non-stationary 1981–2012 AVHRR $NDVI_{3g}$ time series. *Remote Sens. (Basel)* **6**, 6929–6960 (2014).



**Acknowledgments**

**Funding:** This work was funded by the Korea Meteorological Administration Research and Development Program under grant KMI2018-03711. Part of the research was carried out at the Jet Propulsion Laboratory, California Institute of Technology, under a contract with NASA. Part of this research was supported by the Carbon in Arctic Reservoirs Vulnerability Experiment, an Earth Ventures (EV-S1) investigation, under contract with NASA. C.Z. was supported by the National Key R&D Program of China (grant no. 2016YFC0402806). G.S. was supported by the University of Zurich research priority program on Global Change and Biodiversity (URPP GCB). Funding for the MsTMIP (http://nacp.ornl.gov/MsTMIP.shtml) activity was provided through NASA ROSES grant #NNX10AG01A. Data management support for preparing, documenting, and distributing MsTMIP model output data was performed by the Modeling and Synthesis Thematic Data Center at Oak Ridge National Laboratory (ORNL; http://nacp.ornl.gov), with funding through NASA ROSES grant #NNH10AN681. Finalized MsTMIP data products are archived at the ORNL DAAC (http://daac.ornl.gov). This study was part of NASA's Arctic-Boreal Vulnerability Experiment. **Author contributions:** S.-J.J. and A.A.B. designed the research and wrote the majority of the manuscript content. All of the authors discussed the study results and reviewed the manuscript. D.N.H., A.M.M., and C.R.S. provided the MsTMIP data. **Competing interests:** The authors declare that they have no competing interests. **Data and materials availability:** All data needed to evaluate the conclusions in this paper are present in the paper and/or the Supplementary Materials. Additional data related to this paper may be requested from the authors.

Submitted 15 June 2017
Accepted 31 May 2018
Published 11 July 2018
10.1126/sciadv.aao1167

**Citation:** S.-J. Jeong, A. A. Bloom, D. Schimel, C. Sweeney, N. C. Parazoo, D. Medvigy, G. Schaepman-Strub, C. Zheng, C. R. Schwalm, D. N. Huntzinger, A. M. Michalak, C. E. Miller, Accelerating rates of Arctic carbon cycling revealed by long-term atmospheric $CO_2$ measurements. *Sci. Adv.* **4**, eaao1167 (2018).

Science Advances

# Accelerating rates of Arctic carbon cycling revealed by long-term atmospheric $CO_2$ measurements

Su-Jong Jeong, A. Anthony Bloom, David Schimel, Colm Sweeney, Nicholas C. Parazoo, David Medvigy, Gabriela Schaepman-Strub, Chunmiao Zheng, Christopher R. Schwalm, Deborah N. Huntzinger, Anna M. Michalak and Charles E. Miller

*Sci Adv* **4** (7), eaao1167.
DOI: 10.1126/sciadv.aao1167